Korean J. Chem. Eng., **29**(6), 818-822 (2012)
DOI: 10.1007/s11814-011-0233-z

Galvanic corrosion of aluminum alloy (Al2024) and copper in 1.0 M hydrochloric acid solution

Ahmed Y. Musa†, Abu Bakar Mohamad, Ahmed A. Al-Amiery, and Lim Tien Tien

Department of Chemical and Process Engineering, Faculty of Engineering and Built Environment, Universiti Kebangsaan Malaysia, Bangi, 43600, Selangor, Malaysia
(*Received 18 May 2011 • accepted 8 September 2011*)

Abstract–The corrosion of an aluminum alloy (Al2024) and copper in 1.0 M HCl solution was investigated at 30, 40, 50 and 60 °C using open circuit potential (OCP), electrochemical impedance spectroscopy (EIS) and potentiodynamic polarization (PDP) measurements. The galvanic corrosion of Al2024 and copper was studied using the zero resistance ammeter (ZRA) method. Galvanic current densities (I_g) and galvanic potential (E_g) were measured at 30 °C in 1.0 M HCl solution. Thermodynamic parameters, such as activation energy (E_a), enthalpy of activation (ΔH_a) and entropy of activation (ΔS_a), were calculated and discussed. The results indicated that the corrosion rates of both Al2024 and copper increased with temperature. The ZRA results demonstrated that Al2024 is a sacrificial anode in 1.0 M HCl solution when coupled with copper.

Key words: Galvanic Corrosion, Thermodynamic Parameters, ZRA, Copper, Aluminum

INTRODUCTION

Aluminum is an active metal whose resistance to corrosion depends on the formation of the protective oxide film on its surface [1,2]. It is a commercially important metal, and one of its many applications is its frequent use as a reliable and cost-effective sacrificial anode. Aluminum sacrificial anodes are used in major marine projects, e.g., in offshore applications, including structures, platforms, pipelines, jetties and power plants. Aluminum anodes are also used for ship hull and ballast tank protection [3]. Copper is widely used in industry and is often used in the handling of acids. Copper has a high corrosion resistance, and copper alloys possess considerable electrical and heat conductivity, formability, machinability and strength, except at high temperatures. Hydrochloric acid has various usages in industry, e.g., in the pickling of steel and the removal of dust or iron oxide from steel before certain processes. Some industries, like food processing, pharmaceuticals and drinking water, use hydrochloric acid to control the pH of the process water stream. The effects of temperature on the acidic corrosion of aluminum and copper exposed to HCl solutions have been the focus of a substantial number of investigations [4-11].

In general, corrosion rates increase with increasing temperature [12]. For many materials, such as copper, where the oxygen content of the solution directly affects the corrosion rate, the effect of temperature is minimal. In situations where increasing temperatures accelerate the rate of corrosion, the solubility of oxygen is subsequently decreased, and the two effects counteract each other. For other alloys that depend on a passive film for their corrosion resistance, such as aluminum [1,13], the effects of temperature can be pronounced. At elevated temperatures, the soluble oxygen required for repairing the protective oxide film is reduced, and the increased temperatures enhance the reactions that cause the films to break down [14].

In this study, the corrosion behaviors of Al2024 and copper were studied in 1.0 M HCl solution at 30, 40, 50 and 60 °C using open circuit potential (OCP), electrochemical impedance spectroscopy (EIS) and potentiodynamic polarization (PDP) measurements. The galvanic corrosion of Al2024 and copper was studied using the ZRA method.

EXPERIMENTAL SECTION

The working electrodes consisted of Al2024 and copper with active surface areas of 3 cm^2. The composition of Al2024 was (by weight) 3.8% Cu, 0.1% Cr, 0.5% Fe, 1.2% Mg, 0.3% Mn, 0.5% Si, 0.15% Ti and 0.25% Zn, and the balance was Al. The copper electrode was 99.994% pure. The specimens were cleaned according to ASTM standard G1-03 [15]. All measurements were performed in stagnant, non-aerated 1.0 M HCl acid solutions. A Gamry Potentiostat/Galvanostat/ZRA (Ref. 600) was used for the corrosion tests. A three-electrode corrosion cell, with working electrode, graphite counter electrode and saturated calomel electrode (SCE) as the reference electrode, was connected to the Gamry Potentiostat/Galvanostat/ZRA instrument for corrosion measurements. The temperature of the corrosion cell was thermostatically controlled.

The electrochemical cell was allowed to stabilize before performing the electrochemical measurements. The EIS measurements for the Al2024 electrode were performed at the frequencies between 10 kHz and 0.1 Hz, with a signal potential perturbation amplitude of 10 mV. For the copper electrode the frequencies were between 100 kHz to 0.01 Hz, with a signal potential perturbation amplitude of 10 mV. The impedance data were fitted to appropriate equivalent circuits using Gamry Echam Analyst software. The potentiodynamic current-potential curves were obtained by changing the working electrode potential automatically from −200 to 200 mV versus SCE with a scan rate of 0.5 mV s^{-1}. For the galvanic corrosion measure-

†To whom correspondence should be addressed.
E-mail: ahmed.musa@ymail.com, ahmedym@eng.ukm.my

ments, the galvanic current density (I_g) and galvanic potential (E_g) were recorded simultaneously as a function of time using the Gamry Potentiostat/Galvanostat/ZRA instrument and applying a zero potential against the galvanic cell. Al2024 and copper electrodes were installed as a bimetallic shaft (Pine Instruments, Inc, USA) and were immersed in 1.0 M HCl solution for approximately 100 min.

RESULTS AND DISCUSSION

1. Open Circuit Potential (OCP) Measurements

The open circuit potentials for Al2024 and copper are shown in Fig. 1. The OCP values for Al2024 and copper were −712 and −330 mV/SCE, respectively. The OCP values of copper decreased with increasing temperature, whereas the OCP values of Al2024 did not show a clear trend with temperature. Copper's potential was higher than that of Al2024, indicating that the current would flow from copper to Al2024 when coupling in a galvanic corrosion cell [16].

2. Electrochemical Impedance Spectroscopy (EIS) Measurements

Nyquist plots of Al2024 in 1.0 M HCl solution at various temperatures are shown in Fig. 2. The plots show that the impedance decreased with increasing temperature. The impedance spectra consisted of a capacitive loop at high frequencies, followed by an inductive loop at low frequencies. This capacitive loop indicated that a barrier layer was formed on the Al2024 surface, consistent with other literature results that have been reported for aluminum in HCl solution [17,18]. In addition, the capacitive loop is typically related to a charge transfer during the corrosion process and to the formation of an oxide layer on the Al2024 surface. The inductive loop at low frequencies was related to the surface relaxation processes in the oxide film covering the Al2024 surface. The impedance data for Al2024 in 1.0 M HCl solution were fitted using the equivalent circuit model shown in Fig. 3. The circuit consisted of the solution resistance R_s connected in series with the constant phase element CPE_{dl}, which was in parallel with the charge transfer resistance R_{ct} and inductor L, which was connected in series with the layer resistance R_L. CPE was represented as follows [19]:

$$Z(\omega)=Z_0 \cdot j\omega^{-\alpha} \quad (1)$$

where Z_0 is the CPE constant, ω is the angular frequency (rad/s), $j^2=-1$, which is an imaginary number, and α is the CPE exponent [19]. The fitted values of the impedance parameters are listed in Table 1.

The Nyquist plots for copper in 1.0 M HCl solution at selected temperatures are shown in Fig. 4. The impedance spectra were characterized as depressed semicircles at high frequencies that progressed as lines at low frequencies [20]. The same behavior of copper in HCl solution has also been reported in other studies [20,21]. The capacitive loop at high frequencies was due to the charge transfer resistance of copper dissolution, while the diameter of the capacitive loop indicated the magnitude of the charge transfer resistance. The corrosion rate decreased with increasing charge transfer resistance. The high frequency loops were also attributed to the surface

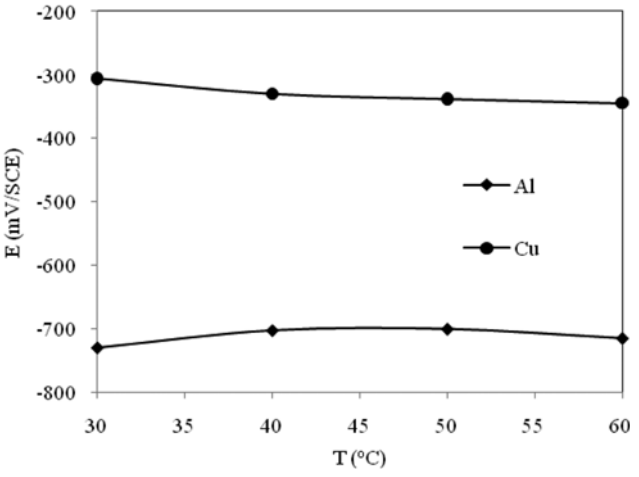

Fig. 1. OCP values as a function of temperature for Al2024 and copper in 1.0 M HCl solution.

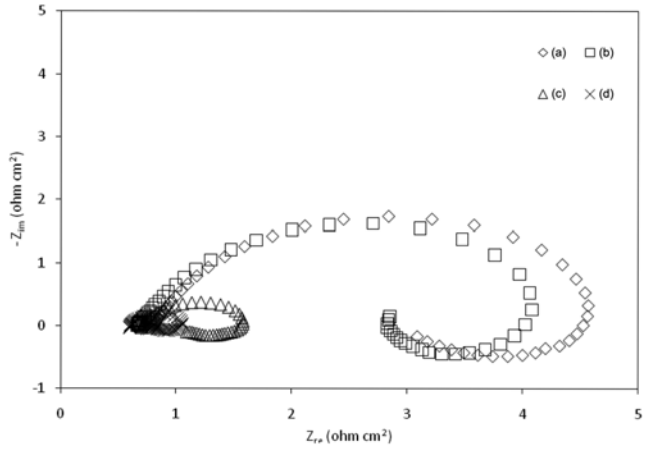

Fig. 2. Nyquist plots for Al2024 in 1.0 M HCl solution at (a) 30, (b) 40, (c) 50 and (d) 60 °C.

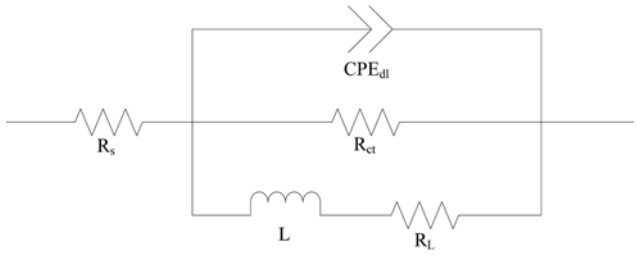

Fig. 3. Equivalent circuit model used to fit Al2024 in 1.0 M HCl solution at various temperatures.

Table 1. Impedance parameters for Al2024 in 1.0 M HCl solution at various temperatures

Temperature (°C)	R_s (ohms cm^2)	L (H cm^2)	R_{ct} (ohms cm^2)	CPE_{dl}	
				$Y_o \times 10^3$ (S s$^\alpha$ cm^{-2})	α
30	0.82	3.41	3.93	2.75	0.89
40	0.68	0.50	4.04	2.97	0.85
50	0.72	0.87	0.85	4.20	0.90
60	0.61	0.38	0.42	3.13	0.96

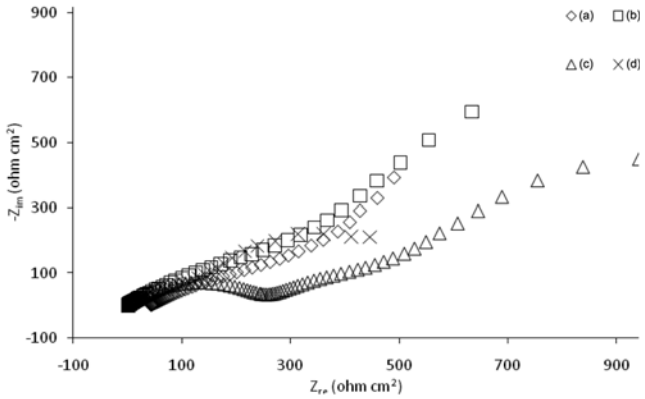

Fig. 4. Nyquist plots for copper in 1.0 M HCl solution at (a) 30, (b) 40, (c) 50 and (d) 60 °C.

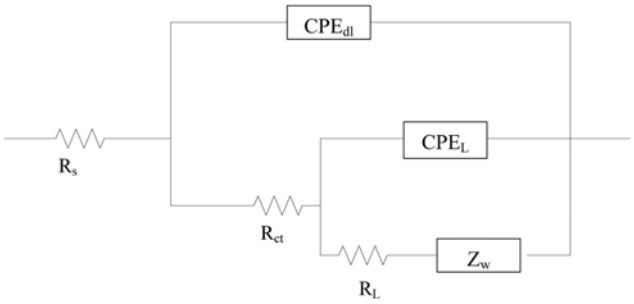

Fig. 5. Equivalent circuit model used to fit copper in 1.0 M HCl solution at various temperatures.

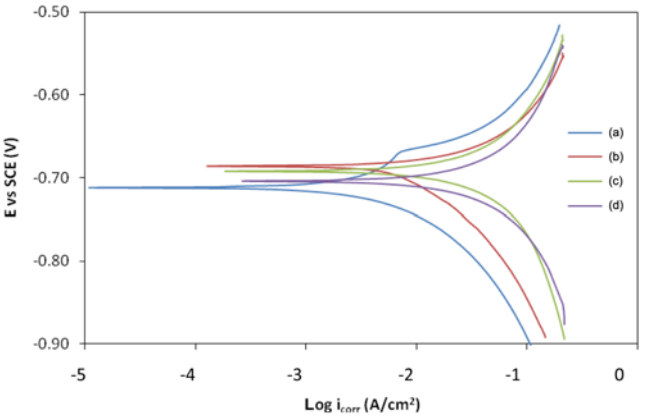

Fig. 6. Potentiodynamic polarization curves for Al2024 in 1.0 M HCl solution at (a) 30, (b) 40, (c) 50 and (d) 60 °C.

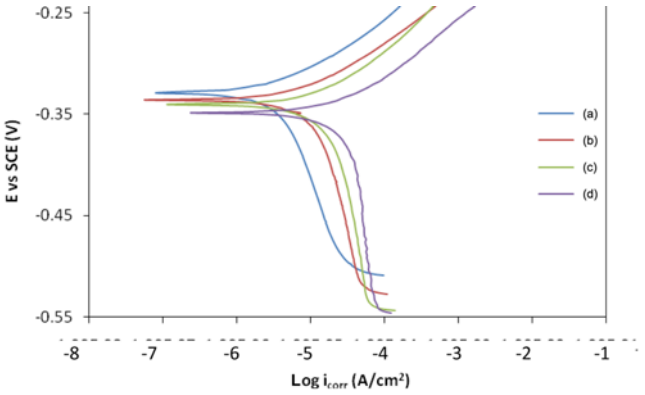

Fig. 7. Potentiodynamic polarization curves for copper in 1.0 M HCl solution at (a) 30, (b) 40, (c) 50 and (d) 60 °C.

relaxation of the copper metal, and the low frequency loops indicated convection and the diffusion mass transport of copper ions [21]. The equivalent circuit model for copper in 1.0 M HCl solution is shown in Fig. 5. It consisted of the solution resistance R_s connected in series with CPE_{dl}, which was in parallel to the charge transfer resistance R_{ct}. The R_{ct} was in series with the surface film capacitance CPE_L and was in parallel with the surface layer resistance R_L, which was in series with the Warburg impedance Z_w. The values of R_{ct} and CPE_{dl} were proposed for the fast charge transfer process of copper dissolution. R_L and CPE_L represented the results of mass transport through the surface film of copper, and Z_w represented the diffusion process. The fitted values of the impedance parameters are tabulated in Table 2.

Tables 1 and 2 indicate that R_{ct} decreased with increasing temperatures, demonstrating that higher temperatures favored the corrosion process. The CPE_{dl} values for Al2024 and copper increased and decreased, respectively, with solution temperature. The Al2024 results implied that the increase in CPE_{dl} values was due to an increase in the local dielectric constant and/or a decrease in the thickness of the electrical double layer, while copper showed the opposite behavior [22].

3. Potentiodynamic Polarization (PDP) Measurements

Polarization curves for Al2024 and copper in 1.0 M HCl solution at the studied temperatures are shown in Fig. 6 and 7, respectively. Both the anodic and cathodic polarization curves increased with temperature, indicating an increase in both the anodic dissolution reaction of the metals and the hydrogen evolution reaction. These results also show that the corrosion current densities of both Al2024 and copper shifted to higher values with increasing solution temperature. The polarization parameters of Al2024 and copper in 1.0 M HCl solution at the selected studied temperatures are in Tables 3

Table 2. Impedance parameters for copper in 1.0 M HCl solution at various temperatures

Temperature (°C)	R_s (ohms cm²)	CPE_{dl}		R_{ct} (ohms cm²)	CPE_L		$Z_W \times 10^3$ (S $s^{1/2}$ cm^{-2})
		Y_o (S s^{α} cm^{-2})	α_1		Y_o (S s^{α} cm^{-2})	α_2	
30	4.14×10^{1}	3.55×10^{-3}	0.43	897.40	8.62×10^{-3}	0.98	1.56
40	8.01×10^{-1}	2.17×10^{-3}	0.57	766.20	1.19×10^{-2}	1.00	1.42
50	1.07×10^{-4}	1.93×10^{-5}	0.61	222.30	1.31×10^{-3}	0.36	3.08
60	4.49×10^{-1}	1.30×10^{-3}	0.71	60.98	5.31×10^{-8}	0.34	8.08

Table 3. Polarization parameters for Al2024 in 1.0 M HCl at various temperatures

Temperature (°C)	β_a (V dec^{-1})	β_c (V dec^{-1})	i_{corr} (mA cm^{-2})	$-E_{corr}$ (mV vs. SCE)	Corrosion rate (mmy)
30	0.15	0.09	5.55	712	58.95
40	0.03	0.10	6.94	686	73.63
50	1.57	1.322	437	693	4640.58
60	2.245	1.151	505	705	5356.86

Table 4. Polarization parameters for copper in 1.0 M HCl at various temperatures

Temperature (°C)	β_a (V dec^{-1})	i_{corr} (μA cm^{-2})	$-E_{corr}$ (mV vs. SCE)	Corrosion rate (mmy)
30	0.04	2.31	328	0.027
40	0.04	4.86	335	0.056
50	0.03	5.15	340	0.060
60	0.06	35.6	348	0.414

and 4, respectively. Table 3 shows that the corrosion current density i_{corr} of Al2024 increased with solution temperature, and a small change was observed in the value of the corrosion potential E_{corr} as the temperature increased. In Table 4, the i_{corr} value for copper increased with solution temperature, while the E_{corr} value became more negative at increased temperatures. The increases in the corrosion rates for both Al2024 and copper were due to the increase in the oxidizing power of the HCl solution at increased temperatures [12].

4. Zero Resistance Ammetry (ZRA) Measurements

The galvanic current density I_g and galvanic potential E_g of Al2024 and copper coupled in 1.0 M HCl solution were recorded for 2 h at 30 °C, as shown in Fig. 8. The current flow from copper to Al2024 was indicated by the electrode potential value. The higher electrode potential of copper over Al2024 prior to coupling made the copper the cathode and the Al2024 the anode. Al2024 formed a thick protective oxide film after it was immersed in HCl solution for 2 h; hence, it became a scarified anode to protect the copper.

The galvanic current behavior exhibited a rapid initial burst, followed by a decrease from 10 to 30 min and then a nearly constant value from 30 to 50 min. It decreased further from 50 to 105 min, but abruptly increased after 105 min. The increase in the galvanic current value during the first stage was due to the rapid corrosion of Al2024 as a result of the galvanic effects with copper. The decrease of the galvanic current value was due to the formation of a passive oxide layer on the Al2024. The galvanic current value finally became constant due to the stabilization of the passive oxide layer of Al2024. Further decreases in the galvanic current value were caused by the hindered dissolution of the metal as a result of the formed passive oxide. The rapid increase in the galvanic current at 105 min was due to the passive oxide layer of Al2024 being damaged [23]. The potential values were in the passive region, which gradually increased to reach about −635 mV [24].

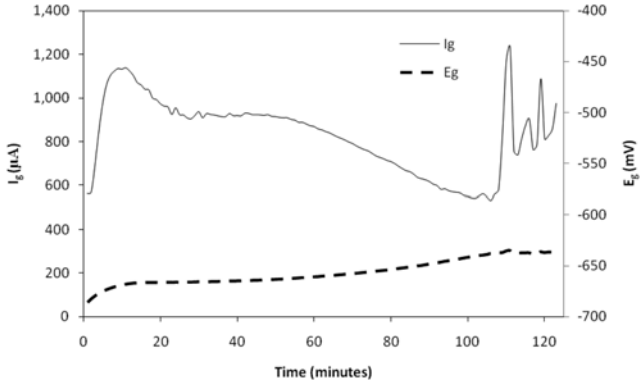

Fig. 8. Galvanic current I_g and galvanic potential E_g as a function of time in 1.0 M HCl solution.

5. Corrosion Kinetic Parameters

The activation energy for the metal corrosion was obtained by the Arrhenius equation as follows:

$$\ln i_{corr} = \left(\frac{-E_a}{R}\right)\left(\frac{1}{T}\right) + \ln A \tag{14}$$

where i_{corr} is the corrosion current in A cm^{-2}, A is the electrochemical constant, E_a is the activation energy in J mol^{-1}, R is the gas constant (8.314 J mol^{-1}K^{-1}) and T is the temperature in K. An Arrhenius plot, the graph of ln i_{corr} against 1000/T, should give a straight line with slope of ($-E_a$/R). Fig. 9 shows the plot for Al2024 and copper in 1.0 M HCl solution, and the E_a values were calculated and are in Table 5. A transition state equation was used to calculate the activation enthalpy ΔH_a and activation entropy ΔS_a:

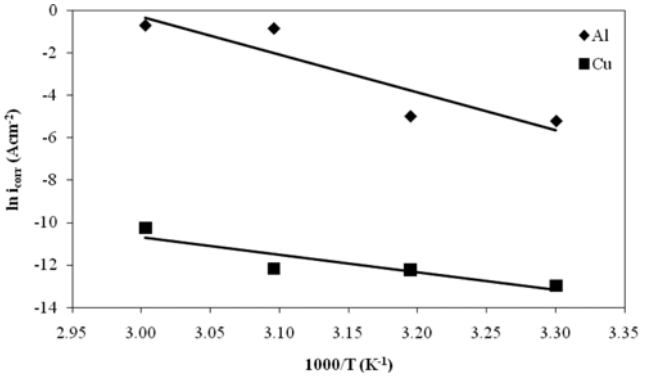

Fig. 9. Arrhenius plots for Al2024 and copper in 1.0 M HCl solution.

Table 5. Corrosion kinetic parameters for Al2024 and copper in 1.0 M HCl at various temperatures

Metal	E_a (kJ mol^{-1})	H_a (kJ mol^{-1})	S_a (J mol^{-1}K^{-1})
Al2024	148.18	145.54	188.55
Copper	68.66	66.02	−136.57

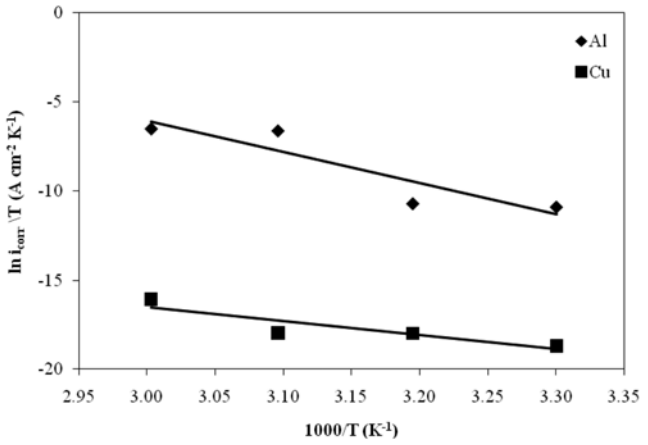

Fig. 10. Transition state plots for Al2024 and copper in 1.0 M HCl solution.

$$\ln\left(\frac{i_{corr}}{T}\right)=\left(\frac{-\Delta H_a}{R}\right)\left(\frac{1}{T}\right)+\left[\ln\left(\frac{R}{Nh}\right)+\frac{\Delta S_a}{R}\right] \quad (16)$$

where N is Avogadro's number, 6.02×10^{23} mol^{-1}, and h is Planck's constant, 6.63×10^{-34} m^2 kg s^{-1}. A plot of ln(i_{corr}/T) against 1000/T should give a straight line with the slope of ($-\Delta H_a$/R) and intercept of [ln(R/Nh)+(ΔS_a/R)], as shown in Fig. 10. ΔH_a and ΔS_a values were calculated for both Al2024 and copper in 1.0 M HCl solution and are in Table 5. The obtained E_a and ΔH_a values were very close to each other. Positive values of ΔH_a for both Al2024 and copper indicated the difficulty of dissolution of these metals in HCl solution [22]. The ΔS_a for Al2024 was positive, while a negative activation entropy value was obtained for copper. The large positive value of ΔS_a for Al2024 indicated the formation of aluminum oxide, Al_2O_3, on the Al2024 surface, while the large negative value of ΔS_a for copper implied that the activated complex, rather than the dissociation step, was the rate-determining step in this reaction.

CONCLUSION

The corrosion behaviors of Al2024 and copper in 1.0 M HCl solution at 30, 40, 50 and 60 °C were studied utilizing open circuit potential (OCP), electrochemical impedance spectroscopy (EIS) and potentiodynamic polarization measurements. The galvanic corrosion of Al2024 and copper coupled in 1.0 M HCl solution at 30 °C was studied using zero resistance ammetry (ZRA). The results indicated that the corrosion rates for both Al2024 and copper increased with increasing solution temperatures. ZRA results demonstrated that Al2024 was the scarified anode when coupled with copper in 1.0 M HCl solution. The corrosion kinetic parameters showed that Al_2O_3 was formed on the surface of the Al2024.

ACKNOWLEDGEMENT

This work was supported by Universiti Kebangsaan Malaysia (Grant no. UKM-GGPM-NBT-037-2011), which is gratefully acknowledged.

REFERENCES

1. V. S. Satri, E. Ghali and M. Elboujdaini, *Corrosion prevention and protection*, John Wiley and Sons, Chichester (2007).
2. S. J. Kim and J. Y. Ko, *Korean J. Chem. Eng.*, **23**, 847 (2006).
3. Gray Pilgrim, 2010, Mild Steel Properties, http://www.buzzle.com/articles/mild-steel-properties.html.
4. S. Ahn, H. J. Song, J. W. Park, J. H. Lee, I. Y. Lee and K. R. Jang, *Korean J. Chem. Eng.*, **27**, 1576 (2010).
5. A. García-Romero, A. Delgado, A. Urresti, K. Martín and J. M. Sala, *Corros. Sci.*, **51**, 1263 (2009).
6. K. F. Khaled, *Corros. Sci*., **52**, 3225 (2010).
7. N. Huynh, S. E. Bottle, T. Notoya and D. P. Schweinsberg, *Corros. Sci*., **42**, 259 (2000).
8. I. B. Obot, N. O. Obi-Egbedi and S. A. Umoren, *Corros. Sci*., **51**, 276 (2009).
9. M. Saenz de Mier, M. Curioni, P. Skeldon and G. E. Thompson, *Corros. Sci*., **50**, 3410 (2008).
10. S. S. Abd El Rehim, M. A. Amin, S. O. Moussa and A. S. Ellithy, *Mater. Chem. Phys*., **112**, 898 (2008).
11. J. C. Rushing and M. Edwards, *Corros. Sci.*, **46**, 1883 (2004).
12. M. G. Fontana, *Corrosion engineering*, McGraw-Hill Book Company, New York (1986).
13. A. Y. Musa, A. A. H. Kadhum, M. S. Takriff and A. B. Mohamad, *Int. J. Surf. Sci. Eng.*, **5**, 226 (2011).
14. http://www.corrosionist.com/effect_temperature_corrosion_chemistry.htm.
15. ASTM G1-3, Standard Practice for Preparing, Cleaning, and Evaluating Corrosion Test Specimens (2003).
16. K. A. Assiongbon, S. B. Emery, V. R. K. Gorantla, S. V. Babu and D. Roy, *Corros. Sci.*, **48**, 372 (2006).
17. S. Yurt, H. Ulutas and H. Dal, *Appl. Surf. Sci.*, **253**, 919 (2006).
18. H. Ashassi-Sorkhabi, B. Shabani, B. Aligholipour and D. Seifzadeh, *Appl. Surf. Sci.*, **252**, 4039 (2006).
19. A. Y. Musa, A. B. Mohamad, A. A. H. Kadhum and Y. B. A. Tabal, *Mater. Eng. Perf.*, **20**, 394 (2011).
20. D. Zhang, Q. Cai, L. Gao and K. Y. Lee, *Corros. Sci.*, **50**, 3615 (2008).
21. L. Larabi, O. Benali, S. M. Mekelleche and Y. Harek, *Appl. Surf. Sci*., **253**, 1371 (2006).
22. A. Y. Musa, A. A. H. Kadhum, A. B. Mohamad, M. S. Takriff, A. R. Daud and S. K. Kamarudin, *Corros. Sci.*, **52**, 526 (2010).
23. M. G. Pujar, N. Parvathavarthini, R. K. Dayal and H. S. Khatak, *Inter. J. Electrochem. Sci.*, **3**, 44 (2008).
24. Z. Zhao and G. S. Frankel, *Corros.*, **63**, 613 (2007).